Research Square

Preprints are preliminary reports that have not undergone peer review.
They should not be considered conclusive, used to inform clinical practice,
or referenced by the media as validated information.

Quantitative CT Perfusion Enhancement Metrics for Differentiating Solid Renal Tumors

Sara Babapour

sara.babapour@yale.edu

University of California, Los Angeles

Jouan Taheri Talesh

University of Alabama at Birmingham

Grace Li

University of California, Los Angeles

Luke Phan

University of California, Los Angeles

Brian Chau

University of California, Los Angeles

James Sayre

University of California, Los Angeles

Research Article

Keywords: Kidney Neoplasms, Renal mass, Quantitative Phase Imaging, CT perfusion, Tumor characterization

Posted Date: May 13th, 2026

DOI: https://doi.org/10.21203/rs.3.rs-9581498/v1

License: This work is licensed under a Creative Commons Attribution 4.0 International License.
Read Full License

Additional Declarations: No competing interests reported.

Abstract

Purpose

Among kidney solid lesions in which neovascularity carries a procedural risk, and benign tumors are prone to overdiagnosis and overtreatment, measurable thresholds may provide reproducible biomarkers to improve diagnostic classification non-invasively. Quantitative contrast distribution metrics, derived from CT perfusion (CTp), were assessed to reflect the solid tumor cytology character.

Method

In this retrospective IRB-approved, HIPAA-compliant study, patients with pathologically confirmed renal masses who underwent CTp imaging prior to interventions were included. Volumes of interest (VOI) were drawn on the most enhancing portion of the mass, ipsilateral and contralateral kidney cortex, after window level adjustments. Maximum HU values relative to wash-in at 0.0 seconds of tissue contrast penetration were obtained on Syngo Via-generated (SH, Malvern, PA) virtually reconstructed image. Relative perfusion parameters of VOI, such as flow extraction (FE), and time to peak (TTP), were compared by a two-sided paired sample t-test between tumors and contralateral cortex and presented as perfusion curves.

Results

A total of 80 target renal lesions were analyzed (ccRCC: N = 44; pRCC: N = 14; oncocytoma: N = 16; Chromophobe: N = 6). Distinctive relative peak wash-in thresholds (HU) for malignant lesions, ccRCC and pRCC ($p < 0.003$; ccRCC-to-cortex > 0.92; pRCC-to-aorta < 0.47) with distinct shorter TTP, or greater peak enhancement for ccRCC were observed compared to healthy cortex ($P < 0.016$). However, both aggressive chromophobe and ccRCC tumors with neovascularity showed overlapping values. Meanwhile, oncocytomas intermediate and indolent enhancement characteristics were presented with distinct washout profiles.

Conclusion

Time- relative enhancement parameters of ccRCC, pRCC are distinctive, and the indolent wash-in curves of benign solid lesions demonstrated remarkable differences in certain hemodynamic parameters.

Introduction

CT and MRI, with one-time per phase image acquisition, have shown satisfactory quality in kidney lesions' differentiation and pathology prediction [1–8] with additional non-invasive and cost-

effectiveness benefits [9]. However, these conventional techniques are prone to time-variability confounding factors in image processing.

On the other hand, integrating human and artificial intelligence to differentiate multiple or binary pathology classifications, an alternative confirmatory merit, requires a precise range of inputs over time for better assistance. Computational features which are feasible inputs for both machine learning models and manual validation have the potential to offer these advantages in clinical settings [10].

CT perfusion (CTp) characterizes tissue hemodynamics by repeatedly sampling attenuation changes following intravenous contrast administration to generate time–attenuation curves. These dynamic profiles obtained over approximately 45–60 seconds with high temporal resolution (sub-second to few-second intervals) allow quantification of perfusion parameters and enable differentiation of hypoperfused and hyperperfused tissue [11, 12].

Functional perfusion parameters are generated based on contrast enhancement, quantified as changes in attenuation measured in Hounsfield units (HU) on CT. This study aims to map neovascular markers of benign and malignant solid (noncystic) renal masses. This effort was to distinguish qualitative flow range differences for differentiation of clear cell renal cell carcinoma (ccRCC) from oncocytoma and the two malignant papillary RCC (pRCC) and chromophobe (chrm) lesions. Identifying predictable patterns in malignant neovascularity and correlating morphologic pathology findings with imaging presentation is a clinical multidisciplinary merit.

Furthermore, quantitative parametric maps can be updated and categorized with the imaging characteristics in cases of a partially necrotic renal tumor, for targeting a pathology in the population and future treatment investigations, or benign lesions' pathognomics, such as oncocytoma with a central scar contrast absorption.

Methods

Study Design and Cohort Selection

This retrospective, HIPAA-compliant, and IRB-approved study utilized a pathology-confirmed kidney lesion database derived from the [Author's institution deleted] imaging system through a CT perfusion keyword search and data query from the integrated diagnostics database. N = 101 patients who underwent excisional or image-guided biopsy of renal lesions between 2018 and 2025 were screened on the imaging archive. Patients' electronic medical records were also manually reviewed for image processing adjustments and readability on pre-procedural CTp using the Syngo Via imaging system (Force, Siemens Healthineers (SH), Erlangen, Germany) for the targeted masses. The limited number of mixed clear-cell papillary subtype cases defined by the recent pathology guideline, and pathology-confirmed angiomyolipoma cases (N = 1), were excluded from analysis, although the enhancement curve figure is included in the supplementary Fig. 1 for benign example presentations. Patients without a

definitive histopathologic diagnosis or without a clearly identifiable lesion on CT perfusion imaging were excluded.

Data selection

80 lesions among patients met the inclusion criteria based on the availability of both diagnostic CT perfusion imaging and corresponding histopathologic confirmation. Lesions of interest were identified on CT, annotated (Fig. 1) and cross-referenced with pathology reports. The index lesions were prospectively reviewed on CT perfusion datasets prior to biopsy, interventional procedures, or treatment initiation to ensure imaging-pathology correlation was implemented without post-procedural confounding elements and consistency across time-resolved perfusion phases. Patients without corresponding pathology reports or without identifiable lesions on pre-procedural CT perfusion imaging were excluded from the study.

Multiple volumes of interest (VOI) were then drawn on the target lesion and the ipsilateral and contralateral healthy cortex, preferably on the posterior aspects and window level adjustments, for the maximum Hounsfield unit data extraction.

Relative perfusion parameters of time to peak (TTP) and peak values (HU) were generated from the perfusion curves normalized to the aorta radiodensity level (Fig. 2). Relative perfusion parameters were compared by a Perfusion parameters were compared by ANOVA between tumors grouped by their pathology reports and by a two-sided paired sample t-test between tumors and the contralateral healthy cortex.

Results

Among 80 selected CTp images with pathology-proven solid renal lesions (average lesion size 2.7 cm), N = 44 ccRCC, N = 14 pRCC, N = 16 oncocytoma, N = 6 Chrm lesions were assessed with CT perfusion.

Relative enhancement metrics demonstrated differential diagnostic performance across tumor subtypes. The shorter lesion TTP compared to the contralateral cortex significantly distinguished ccRCC from oncocytoma and pRCC ($p < 0.003$), while a greater peak ccRCC radiodensity HU value in correlation to the contralateral cortex further improved discrimination between ccRCC and all other subtypes ($p < 0.001$, Fig. 3). A maximum lesion-to-cortex contrast ratio greater than 0.92 was observed in 77.3% of ccRCC cases (34/44; 95% CI: 62.8%–87.7%) with an earlier lesion peak (shorter TTP) in comparison to cortex. Invasive hypervascular cases of chromophobe showed overlapping values for the remaining undifferentiated cases.

Low peak lesion enhancement (nearly comparable to cysts Fig. 4) was observed in pRCC, with a maximum lesion-to-aorta contrast ratio < 0.47 in 96% of cases (95% CI: 72.5%–99.5%). Benign indolent

wash-in characteristic in the corticomedullary phase is discrete in the generated graphs (supplementary Fig. 1, Fig. 5).

Discussion

This investigation offers several insights into current literature validation. Time-resolved blood flow and wash-in features in this study provided additional classification value to kidney solid lesion subtypes. ccRCC exhibited shorter TTP (within 10–30 seconds post-contrast injection) compared to the same level renal cortex, consistent with hypervascular malignant lesions. In contrast, oncocytomas demonstrated either delayed TTP or lower peak enhancement values relative to the same level healthy cortex radiodensity, despite occasional overlap with ccRCC in absolute radiodensities. pRCC showed consistently low enhancement, reflecting its hypovascular cell type architecture. Nevertheless, invasive chromophobe RCC (supplementary Fig. 2) demonstrated occasional unremarkable overlapping enhancement characteristics with ccRCC in absolute measures, limiting differentiation based on peak intensity alone.

This CT perfusion database also uniquely reveals the optimum wash-in time to discern lesions with hypervascularity as a pathognomic sign. Distinct low lesion values in pRCC lesions, while indolent (lower and slow) TTP in benign and hypovascular solid lesions, are key to manual assessment. The enhancement curve profiling in CTp is clinically useful for visualizing lesions characteristic compared to the baseline healthy cortex area qualitatively. TTP can mainly be utilized when the heterogeneous appearance and overlapping high signal intensity are indistinct between oncocytoma and clear cell lesions [13].

Since this study targeted pathology nature of lesions above any other markers, results may be reliable and reproducible within each commercial software.

Limitations to this assessment are similar to those of other CT evaluations. Depending on the kinetic model, pCT can be significantly more susceptible to motion artifact and noise with a large body habitus. Though as CTp technology improves, perfusion imaging may supplant regular contrast CT for certain indications, including oncology and functional assessment.

Parallel to literature clinical guideline updates[14–16], prior studies have also demonstrated absolute and relative attenuation utility in the solid renal lesions separately on wash-out phases [17, 18] and on triple-phase examinations [6, 19–21]. Among all these studies, one-time acquisition was obtained per phase but was extensively described in this study within the corticomedullary-to-nephrogenic phase, with wash-in curve illustrations per time. This technique may play a complementary role to the patient's clinical assessment, with contraindications to invasive procedures and challenging conditions[22].

Conclusion

Quantitative CT perfusion–derived enhancement metrics provide valuable noninvasive biomarkers for differentiating renal tumor subtypes. These parameters may improve preoperative characterization of renal masses and assist in clinical decision-making. Significant differences were demonstrated in time-to-peak and one-time maximum HU value among ccRCC and pRCC and oncoytoma compared to healthy cortex. Utilizing relative time-to-peak enhancement and maximum contrast concentration compared to the kidney cortex and aorta assists in tumor pathology characterization in the majority of prevalent solid renal lesions.

Time-relative CT perfusion parameters differ by renal mass histological subtype and may help characterize the pathology of frequent solid renal lesions, utilizing lesion time to peak and peak enhancements compared to the kidney cortex.

Declarations

Ethics approval

This retrospective study was approved by the local Institutional Review Board (IRB) and was conducted in accordance with the ethical standards of the Declaration of Helsinki and its later amendments.

Consent to participate

The requirement for informed consent to participate was waived by the IRB due to the retrospective nature of the study and the use of de-identified data.

Competing interests

The authors declare that they have no relevant financial or non-financial competing interests to disclose.

Author Contribution

Conception or design of the work: Jouan Taheri Talesh, Sara Babapour, Brian ChauData acquisition and draft preparation: Luke Phan, Grace Li, Sara BabapourAnalysis and interpretation of data: James Sayre, Sara BabapourIntellectual content and accountable for all aspects of the work: Sara Babapour

Acknowledgement

The authors acknowledge support from the Radiology Department at UCLA and Dr. Raman's clinical research lab and thank the IDx data management teams for their unwavering support.

Data availability

The datasets generated and/or analyzed during the current study are not publicly available due to patient privacy and institutional restrictions but are available from the corresponding author on reasonable request and with approval from the appropriate institutional authorities.

References

1. Shetty AS, Fraum TJ, Ballard DH, Hoegger MJ, Itani M, Rajput MZ, et al. Renal Mass Imaging with MRI Clear Cell Likelihood Score: A User's Guide. Radiographics. 2023;43(7):e220209. doi: 10.1148/rg.220209.
2. Johnson BA, Kim S, Steinberg RL, de Leon AD, Pedrosa I, Cadeddu JA. Diagnostic performance of prospectively assigned clear cell Likelihood scores (ccLS) in small renal masses at multiparametric magnetic resonance imaging. Urol Oncol. 2019;37(12):941–6. doi: 10.1016/j.urolonc.2019.07.023.
3. Dunn M, Linehan V, Clarke SE, Keough V, Nelson R, Costa AF. Diagnostic Performance and Interreader Agreement of the MRI Clear Cell Likelihood Score for Characterization of cT1a and cT1b Solid Renal Masses: An External Validation Study. AJR Am J Roentgenol. 2022;219(5):793–803. doi: 10.2214/AJR.22.27378.
4. Blachura T, Matusik PS, Kowal A, Radzikowska J, Jarczewski JD, Skiba L, et al. Diagnostic accuracy of the Clear Cell Likelihood Score and selected MRI parameters in the characterization of indeterminate renal masses - a single-institution study. Abdom Radiol (NY). 2024;49(11):3893–901. doi: 10.1007/s00261-024-04484-5.
5. Al Nasibi K, Pickovsky JS, Eldehimi F, Flood TA, Lavallee LT, Tsampalieros AK, et al. Development of a Multiparametric Renal CT Algorithm for Diagnosis of Clear Cell Renal Cell Carcinoma Among Small (</= 4 cm) Solid Renal Masses. AJR Am J Roentgenol. 2022;219(5):814–23. doi: 10.2214/AJR.22.27971.
6. Lee-Felker SA, Felker ER, Tan N, Margolis DJ, Young JR, Sayre J, et al. Qualitative and quantitative MDCT features for differentiating clear cell renal cell carcinoma from other solid renal cortical masses. AJR Am J Roentgenol. 2014;203(5):W516–24. doi: 10.2214/AJR.14.12460.
7. Patel HD, Huai K, Elliott N, Thorson DL, Rac G, Picken MM, et al. Differentiating Oncocytic Renal Tumors from Chromophobe Renal Cell Carcinoma: Comparison of Peak Early-phase Enhancement Ratio to Clinical Risk Factors and Rater Predictions. Eur Urol Open Sci. 2022;46:8–14. doi: 10.1016/j.euros.2022.10.006.
8. Zhang J, Lefkowitz RA, Ishill NM, Wang L, Moskowitz CS, Russo P, et al. Solid renal cortical tumors: differentiation with CT. Radiology. 2007;244(2):494–504. doi: 10.1148/radiol.2442060927.
9. Chen KY, Lange MJ, Qiu JX, Lambert D, Mithqal A, Krupski TL, et al. Cost-Effectiveness Analysis of the Clear Cell Likelihood Score Against Renal Mass Biopsy for Evaluating Small Renal Masses. Urology. 2024;188:111–7. doi: 10.1016/j.urology.2024.04.007.
10. Karhi S, Tahtinen O, Aherto J, Matikka H, Manninen H, Nerg O, et al. Effect of different thresholds for CT perfusion volumetric analysis on estimated ischemic core and penumbral volumes. PLoS One. 2021;16(4):e0249772. doi: 10.1371/journal.pone.0249772.

11. Wintermark M, Smith WS, Ko NU, Quist M, Schnyder P, Dillon WP. Dynamic perfusion CT: optimizing the temporal resolution and contrast volume for calculation of perfusion CT parameters in stroke patients. AJNR Am J Neuroradiol. 2004;25(5):720–9.
12. Konstas AA, Goldmakher GV, Lee TY, Lev MH. Theoretic basis and technical implementations of CT perfusion in acute ischemic stroke, part 1: Theoretic basis. AJNR Am J Neuroradiol. 2009;30(4):662–8. doi: 10.3174/ajnr.A1487.
13. Cha D, Kim CK, Park JJ, Park BK. Evaluation of hyperdense renal lesions incidentally detected on single-phase post-contrast CT using dual-energy CT. Br J Radiol. 2016;89(1062):20150860. doi: 10.1259/bjr.20150860.
14. Ward RD, Tanaka H, Campbell SC, Remer EM. 2017 AUA Renal Mass and Localized Renal Cancer Guidelines: Imaging Implications. Radiographics. 2018;38(7):2021–33. doi: 10.1148/rg.2018180127.
15. Motzer RJ, Jonasch E, Agarwal N, Bhayani S, Bro WP, Chang SS, et al. Kidney Cancer, Version 2.2017, NCCN Clinical Practice Guidelines in Oncology. J Natl Compr Canc Netw. 2017;15(6):804–34. doi: 10.6004/jnccn.2017.0100.
16. Expert Panel on Urologic I, Wang ZJ, Nikolaidis P, Khatri G, Dogra VS, Ganeshan D,et al. ACR Appropriateness Criteria® Indeterminate Renal Mass. Journal of the American College of Radiology. 2020;17(11):S415–S28. doi: 10.1016/j.jacr.2020.09.010.
17. Nicolau C, Bunesch L, Pano B, Salvador R, Ribal MJ, Mallofre C, et al. Prospective evaluation of CT indeterminate renal masses using US and contrast-enhanced ultrasound. Abdom Imaging. 2015;40(3):542–51. doi: 10.1007/s00261-014-0237-3.
18. Corwin MT, Altinmakas E, Asch D, Bishop KA, Boge M, Curci NE, et al. Clinical Importance of Incidental Homogeneous Renal Masses That Measure 10–40 mm and 21–39 HU at Portal Venous Phase CT: A 12-Institution Retrospective Cohort Study. AJR Am J Roentgenol. 2021;217(1):135–40. doi: 10.2214/AJR.20.24245.
19. Mileto A, Marin D, Ramirez-Giraldo JC, Scribano E, Krauss B, Mazziotti S, et al. Accuracy of contrast-enhanced dual-energy MDCT for the assessment of iodine uptake in renal lesions. AJR Am J Roentgenol. 2014;202(5):W466–74. doi: 10.2214/AJR.13.11450.
20. Marin D, Davis D, Roy Choudhury K, Patel B, Gupta RT, Mileto A, et al. Characterization of Small Focal Renal Lesions: Diagnostic Accuracy with Single-Phase Contrast-enhanced Dual-Energy CT with Material Attenuation Analysis Compared with Conventional Attenuation Measurements. Radiology. 2017;284(3):737–47. doi: 10.1148/radiol.2017161872.
21. Ascenti G, Mileto A, Krauss B, Gaeta M, Blandino A, Scribano E, et al. Distinguishing enhancing from nonenhancing renal masses with dual-source dual-energy CT: iodine quantification versus standard enhancement measurements. Eur Radiol. 2013;23(8):2288–95. doi: 10.1007/s00330-013-2811-4.
22. Liu X, Zhou J, Zeng MS, Ma Z, Ding Y. Homogeneous high attenuation renal cysts and solid masses–differentiation with single phase dual energy computed tomography. Clin Radiol. 2013;68(4):e198–205. doi: 10.1016/j.crad.2012.11.008.

Figures

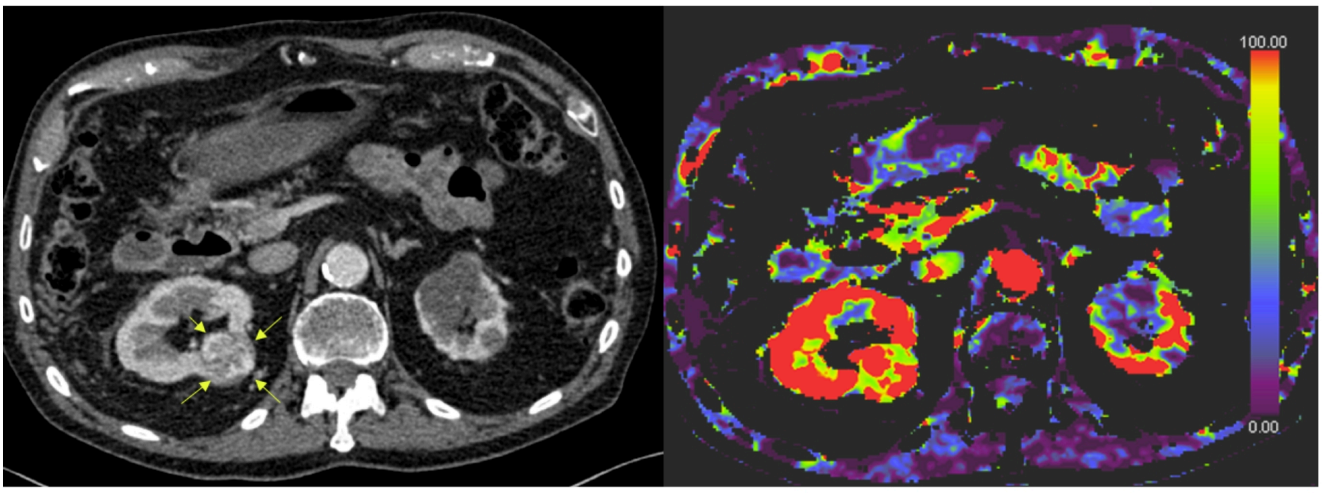


Figure 1

An annotated ccRCC lesion on CTp temporal average and perfusion sequences with a generated curve on Syngo Via is depicted in this image

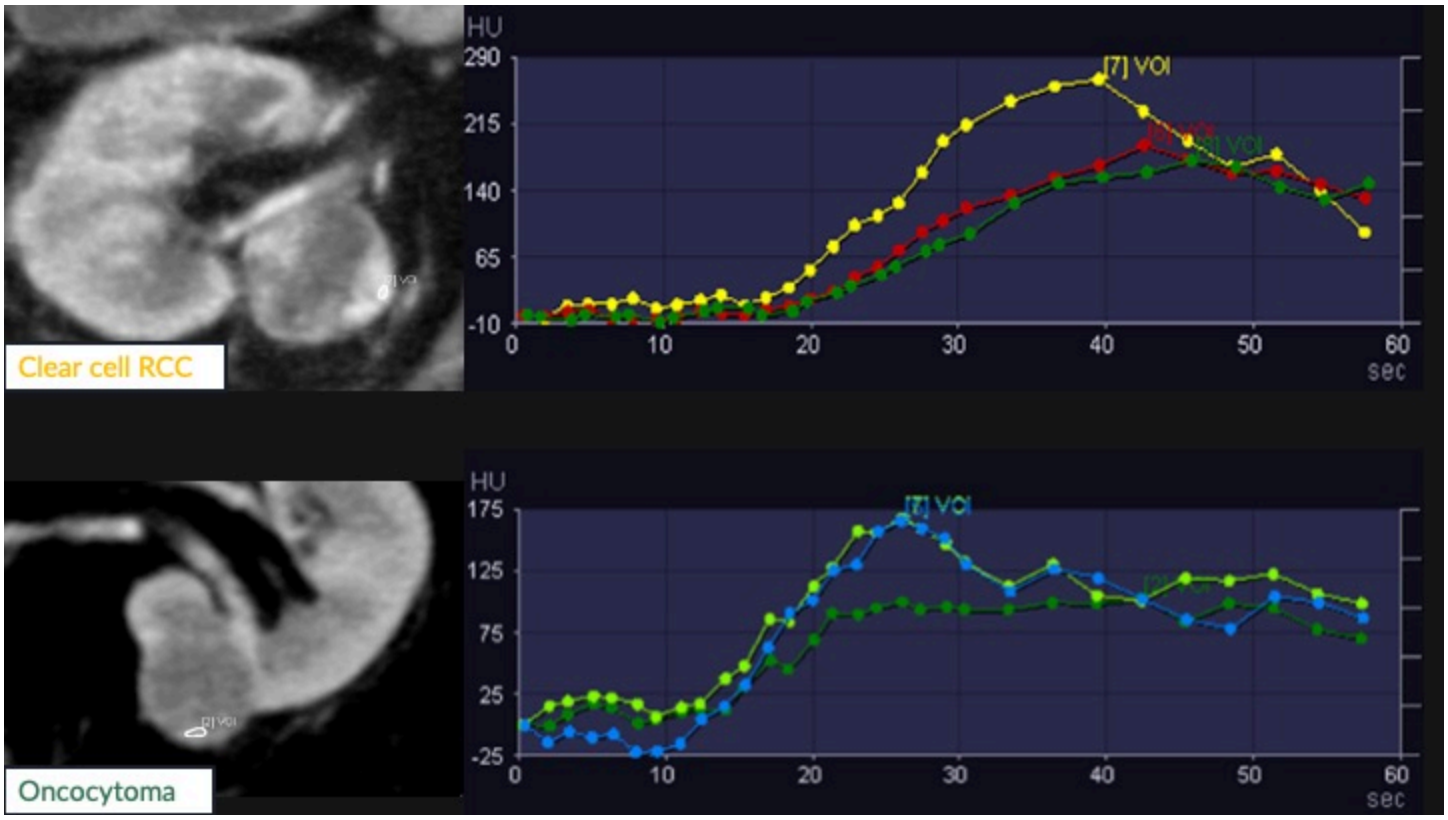
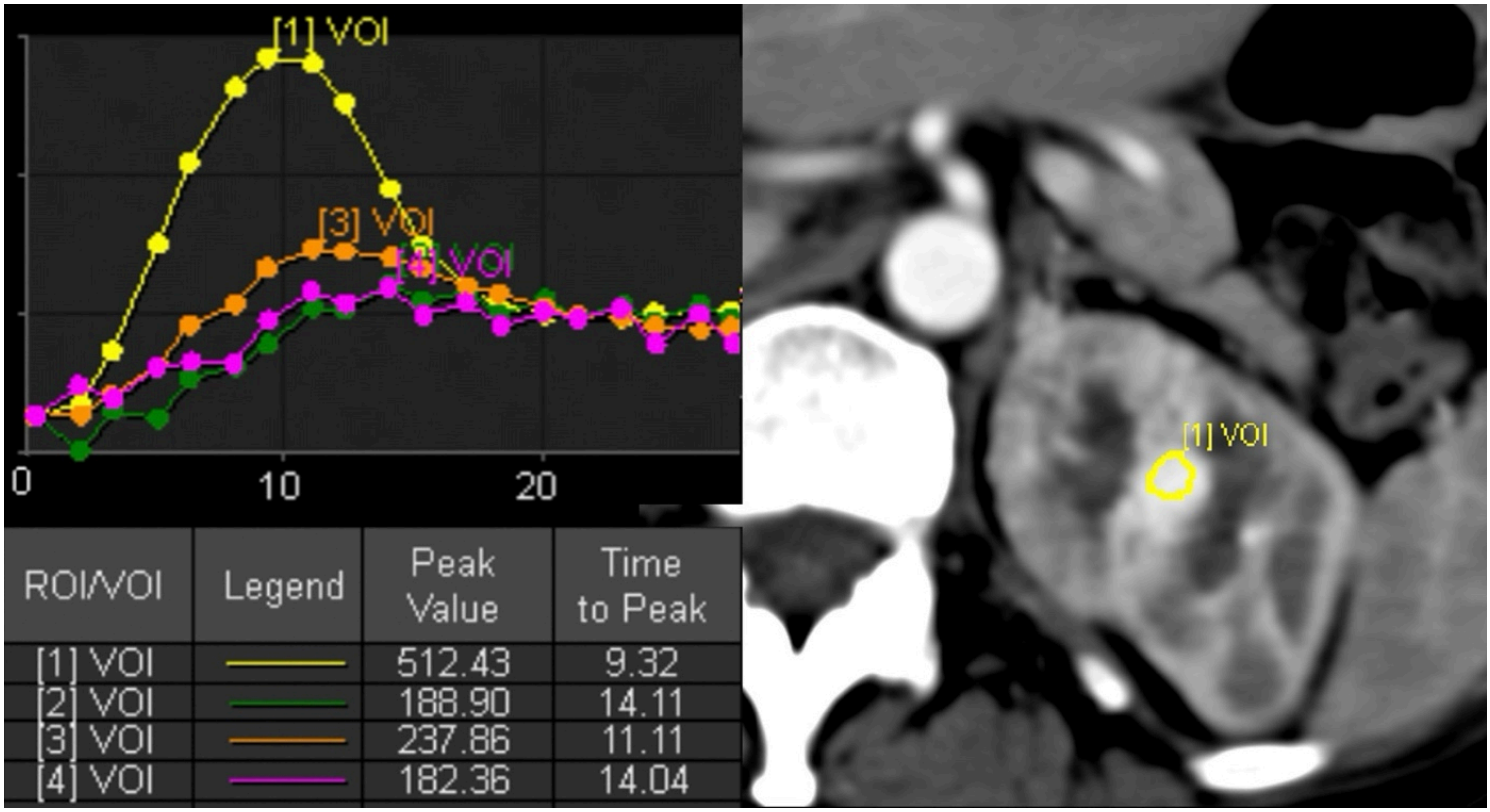


Figure 2

Presenting the commercial Syngo Via application view on different peak enhancement patterns between benign (VOI 2 in oncocytoma) and malignant (VOI 7 in ccRCC) renal lesions before image pre-processing (The average vessel enhancement processing for time-relative values was not adjusted in this image).



ROI/VOI	Legend	Peak Value	Time to Peak
[1] VOI		512.43	9.32
[2] VOI		188.90	14.11
[3] VOI		237.86	11.11
[4] VOI		182.36	14.04

Figure 3

A 78-year-old male with a T1b stage ccRCC malignant lesion (VOI 1 and VOI 3), showing a rapid peak enhancement value chart extracted from syngo.via beyond the ipsilateral kidney cortex (VOI 2) and the contralateral cortex (VOI 4), maximum values. The X and Y axes demonstrate time (seconds) and radiodensity (HU) in the curve graph, respectively.

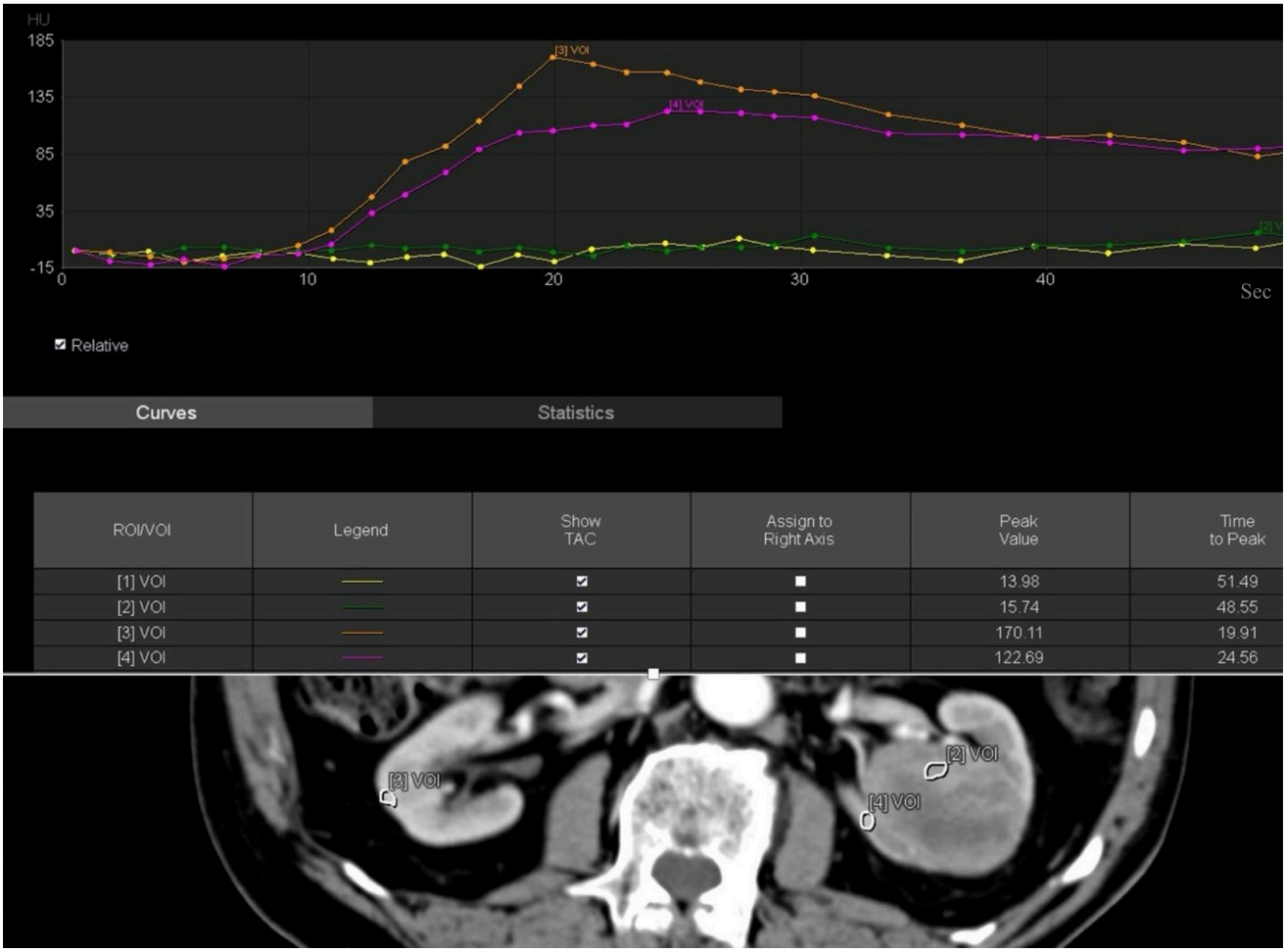


Figure 4

Low papillary renal cell carcinoma lesion enhancement quantification on syngo.via. Both VOI 1 and 2 (yellow and green) were obtained on the lesion for better assessment, whereas VOI 4 (purple) is presented on the ipsilateral and VOI 3 (orange) on the contralateral kidney cortex. This figure is a direct file export presentation from syngo.via.

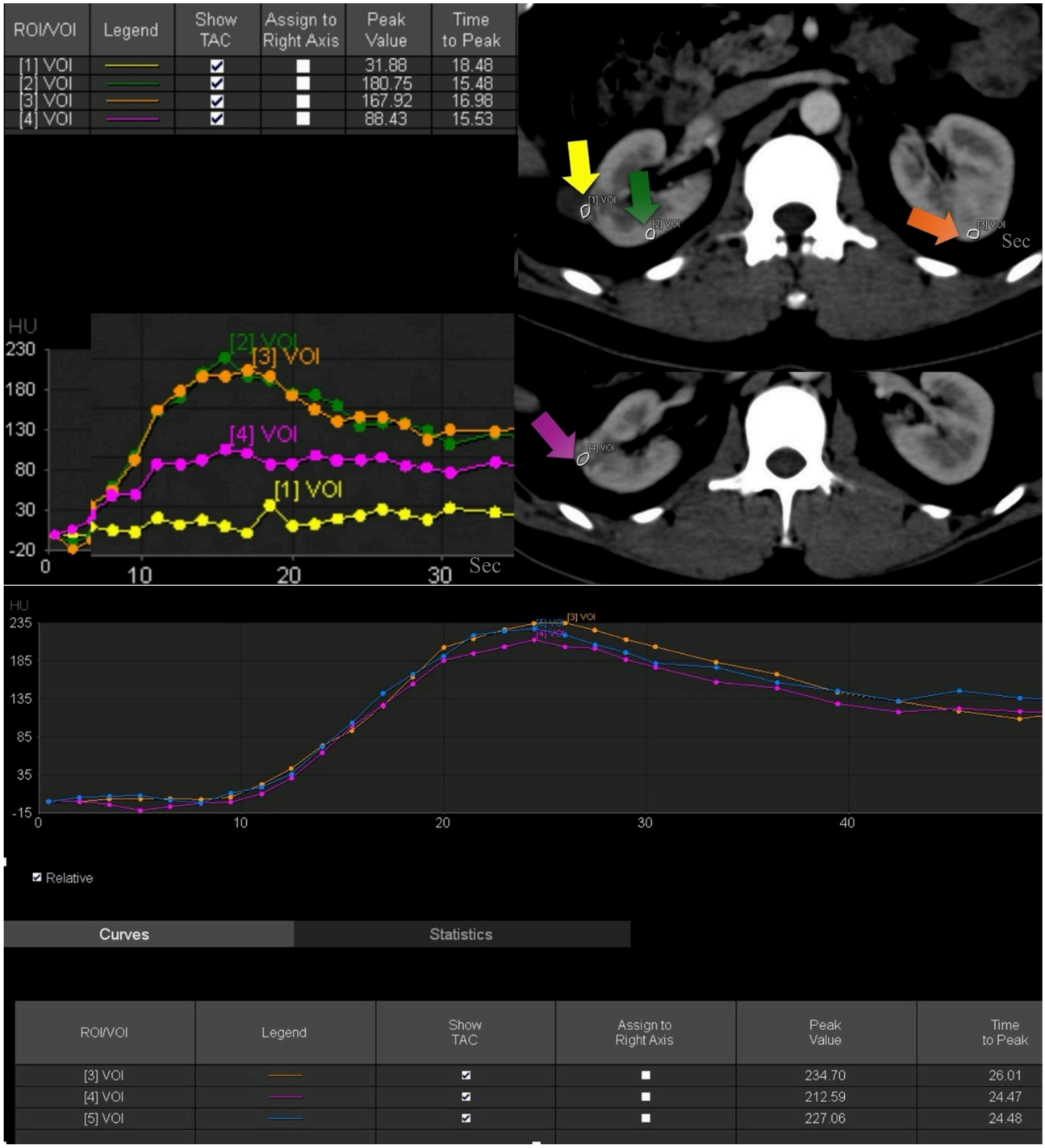


Figure 5

Two oncocytoma lesion presentations on syngo.via. Top figure (VOI 1 yellow signs) and VOI 4 purple signs were two attempts in different CT slices to extract maximum lesion enhancement, while VOI 2 is ipsilateral and VOI 3 is contralateral) shows throughout lower maximum enhancement pattern compared to cortex, similar to benign lesions, while the bottom figure is a peak enhancement pattern (orange VOI 3) similar to ccRCC with a delayed lesion peak compared to kidney cortex (purple VOI 4 and blue 5).

Maximum cortex-enhancement flow was observed in the posterior aspects of the kidneys. All quantitative values are presented in relative values at the starting points (values were subtracted from before contrast penetrated the kidneys at 0.0 seconds).

Supplementary Files

This is a list of supplementary files associated with this preprint. Click to download.

- floatimage6.jpeg
- floatimage7.jpeg